Electrochimica Acta 54 (2009) 4371–4377

Contents lists available at ScienceDirect

Electrochimica Acta

journal homepage: www.elsevier.com/locate/electacta

The role of *in situ* generated nano-sized metal particles on the coulombic efficiency of $MGeO_3$ (M = Cu, Fe, and Co) electrodes

Chang H. Kim, Yoon S. Jung, Kyu T. Lee, Jun H. Ku, Seung M. Oh*,[1]

Department of Chemical and Biological Engineering, and Research Centre for Energy Conversion & Storage, Seoul National University, Seoul 151-744, South Korea

ARTICLE INFO

Article history:
Received 4 September 2008
Received in revised form 5 March 2009
Accepted 6 March 2009
Available online 19 March 2009

Keywords:
Lithium ion batteries
Anode
Metal oxide electrodes
Nano-sized metal particles
Coulombic efficiency

ABSTRACT

To improve the coulombic efficiency of GeO_2 electrode, a Cu-containing ternary metal oxide ($CuGeO_3$) was prepared and the electrochemical behavior of Cu component was studied. The GeO_2 electrode shows a low coulombic efficiency in the first cycle (43%), which is mainly caused by a poor Ge oxidation kinetics ($Ge + 2Li_2O \rightarrow GeO_2 + 2Li^+ + 2e^-$). The X-ray absorption spectroscopy (XAS) data illustrate that the Cu component in $CuGeO_3$ is converted to nano-sized metallic Cu in the earlier stage of lithiation but idles thereafter. In contrast, the Ge component in $CuGeO_3$ behaves like the GeO_2 electrode. It is converted to nano-sized Ge by a conversion reaction and further lithiated by alloying reaction. The de-lithiation proceeds in the reverse order. The $CuGeO_3$ electrode shows a much improved coulombic efficiency (74%) in the first cycle, which is indebted to a facilitated Ge oxidation with a much reduced electrode polarization. This feature has been explained by the favorable roles provided by the *in situ* generated nano-sized metallic Cu particles that make such an intimate contact with the nano-sized Ge and Li_2O that they can catalyze Li_2O decomposition and provide an electronic conductive network for Ge oxidation. A similar favorable effect was observed with the other ternary oxides ($FeGeO_3$ and $CoGeO_3$), wherein the formation of nano-sized metallic Fe and Co can be assumed.

1. Introduction

Recently, metal oxide electrodes such as CoO, NiO, SnO_2, and GeO_2 have received a much attention since they possess a higher theoretical capacity than that of graphites [1–5]. Such a high capacity can be assumed since they are lithiated by a conversion-type reaction with more than one-electron reduction (for instance, $CoO + 2Li^+ + 2e \rightarrow Co + Li_2O$), which is contrasted by the conventional electrodes that are lithiated by less than one-electron reduction (for instance, graphites). Even higher theoretical capacity is expected if the metal components are further lithiated by alloying reaction with Li. For instance, GeO_2 is lithiated by a conversion reaction ($GeO_2 + 4Li^+ + 4e \rightarrow Ge + 2Li_2O$) and the elemental-state Ge is further lithiated by an alloying reaction ($Ge + xLi^+ + xe \rightarrow Li_xGe$) [5].

In practice, the metal oxides have not been used as an electrode for lithium secondary batteries since they have many problems to be solved [1–6]. They show a large hysteresis between charge and discharge voltage. A severe volume change with cycling is another problem. Finally, a large irreversible capacity (low coulombic efficiency) evolved in the first cycle, which is caused by an incomplete de-lithiation reaction (oxidation of metallic component/Li_2O decomposition, for instance, $Co + Li_2O \rightarrow CoO + 2Li^+ + 2e$), is another problem. To solve or at least alleviate the irreversibility problem, broadly two approaches have been made in the literature. The first approach concerns a minimization of electrochemical Li_2O formation. This idea is based on the fact that the heterogeneous reaction between metal (for instance, Co) and Li_2O particles is intrinsically slow, such that the Li consumed for Li_2O formation is not fully recovered in the forthcoming de-lithiation process [7–9]. In this circumstance, the amount of Li remained as Li_2O appears as an irreversible capacity. The typical example of this approach is the work performed by Nam et al. [8]. They prepared a SnO_2 thin-film electrode, onto which Li metal was deposited. During the next heat-treatment period, the SnO_2 is converted to metallic Sn and Li_2O, such that there is no Li consumption for electrochemical Li_2O formation. The second approach is to incorporate an extra metallic component to facilitate the solid-state reaction between metal and Li_2O [10–13]. For instance, Kang et al. reported that the coulombic efficiency of Co_3O_4 electrode is greatly increased by adding metallic Ni by high-energy ball milling [10]. As the roles of this extra metallic component (Ni), the following has been proposed: (i) electrocatalyst for Li_2O decomposition, (ii) electronic conductive network formation between metallic Co and Li_2O to facilitate the Co oxidation, and (iii) buffering matrix to minimize the volume change associated with a lithiation of Co_3O_4.

This work is an extension of the second approach since we add an extra metallic component in metal oxide electrode, but the

* Corresponding author. Tel.: +82 2 880 7074; fax: +82 2 872 5755.
E-mail address: seungoh@snu.ac.kr (S.M. Oh).
[1] ISE member.

0013-4686/$ – see front matter © 2009 Elsevier Ltd. All rights reserved.
doi:10.1016/j.electacta.2009.03.009

difference to the previous approaches is the *in situ* generation of metal particles by cell cycling. As a model compound, we have chosen the ternary metal oxides ($MGeO_3$, where M = Cu, Fe and Co) with the following expectations in mind. First, the extra metal components (M) are converted to their elemental state by a conversion reaction, thereby they can play the roles that have been proposed in the previous literature. This idea has been developed on the basis of the fact that the reduction potential of Cu(II), Fe(II) and Co(II) is higher than that for Ge(IV), such that the metal particles (M) are generated before the Ge(IV) reduction and remain in their metallic state until the metallic Ge is oxidized [5,14]. Second, the extra metal components (M) are converted to nano-sized particles, which seem to be very likely since the electrochemical reduction takes place within an $MGeO_3$ particle in an atomic scale. If this is the case, the nano-sized metal particles can play the proposed roles more effectively than the bulkier metal particles employed in the previous works.

2. Experimental

2.1. Preparation and characterization of materials

A series of crystalline $MGeO_3$ (M = Cu, Fe and Co) powder (0.5–10 μm) was prepared by solid-state reaction with GeO_2 powder (99.998%, Aldrich, 0.5–5 μm), CuO (Aldrich, 20–300 nm), Fe_2O_3 (99+%, Aldrich, <5 μm), and CoO (Aldrich, 325 mesh). The corresponding powders were mixed in a stoichiometric ratio and sealed in a steel bowl. After high-energy ball-milling for 4 h, the mixture was pressed into a pellet under 3000 psi for 10 min, which was followed by heat-treatment at 1000 °C for 12 h in air. For a control experiment, the CuO/GeO_2 sample was prepared by high-energy ball-milling of CuO/GeO_2 mixture (1:1 atomic ratio). The X-ray diffraction (XRD) data of ternary oxides were indexed with; $CuGeO_3$: JCPDS #01-089-9047, $FeGeO_3$: JCPDS #00-035-1265, and $CoGeO_3$: JCPDS #00-017-0814.

XRD patterns were obtained with a RIGAKU D/MAX-2500-PC equipped with Cu Kα radiation (1.54056 Å). The Ge K-edge and Cu K-edge X-ray absorption spectroscopy (XAS) and extended X-ray absorption fine structure (EXAFS) data were obtained at the Pohang Light Source (PLS) with a ring current of 120–170 mA at 2.5 GeV. Data were collected in a transmission mode using gas-filled ionization chambers (30% nitrogen and 70% argon) as detectors. A Si (1 1 1) monochromator crystal was used with detuning to 80% in intensity to eliminate the high-order harmonics. Energy calibration for Ge K-edge and Cu K-edge was carried out using Ge and Cu powder, respectively. For the XRD and XAS analysis, the cells were disassembled in Ar-filled dry box and the current collector was removed from the electrode. Disassembled electrode was coated with polyimide (KAPTON) film to prevent oxidation.

2.2. Electrochemical characterization

The composite electrodes were prepared by spreading a slurry mixture of metal oxide powder, poly(vinylidene fluoride) (PVdF, as a polymer binder), and carbon additive (super P, for conductivity enhancement) (7:1.5:1.5 weight ratio) on a piece of Cu foil. Li metal foil was used as the counter electrode. The used electrolyte was 1.0 M $LiPF_6$ dissolved in a mixture of ethylene carbonate (EC) and dimethyl carbonate (DMC) (1:1 volume ratio). Electrochemical tests were performed with a two-electrode 2032-type coin cell in the potential range of 0.01–3.00 V (vs. Li/Li^+) at 25 °C. Galvanostatic charge/discharge cycling was made at a current density of 100 mA g^{-1}. Cyclic voltammograms were recorded at a scan rate of 20 μV s^{-1}. In this report, the lithiation was expressed as discharging, whereas the de-lithiation charging.

3. Results and discussion

3.1. Lithiation/de-lithiation mechanism of $CuGeO_3$ electrode

The first discharge–charge voltage profile of $CuGeO_3$/Li cell is presented in Fig. 1a. The $CuGeO_3$ electrode is lithiated up to 9.34 Li/Ge and de-lithiated by 6.92 Li/Ge in the first cycle. The coulombic efficiency is calculated to be 74%. The voltage plateaus appeared at 1.7 V and near 0.0 V in the lithiation, and those at 0.5 V, 1.2 V and 1.8 V in the de-lithiation are well-matched with the current peaks appeared in the cyclic voltammogram (Fig. 1b).

In order to trace the lithiation/de-lithiation pathway for $CuGeO_3$ electrode, the Cu K-edge and Ge K-edge XANES and EXAFS spectra were obtained (Fig. 2). For a referencing purpose, the spectra for CuO, Cu, GeO_2 and Ge are provided in the inset. As shown in Fig. 2a, the Cu K-edge XANES spectrum of initial $CuGeO_3$ looks very close to that for the CuO reference (scan #1), implying that the oxidation state of Cu in $CuGeO_3$ is close to two. When lithiation proceeds across the voltage plateau appeared at 1.7 V (scan #2–3), the Cu component is reduced to its metallic state as evidenced by the similarity between the spectrum (scan #3) and that for the Cu reference. The other spectra (scan #4–6) in Fig. 2a strongly suggest that the Cu component remains as an elemental state thereafter. The earlier reduction of Cu component in $CuGeO_3$ is further evidenced by the Cu K-edge EXAFS spectra shown in Fig. 2c, where it is seen that the intensity of Cu–Cu bond sharply increases in the earlier stage of

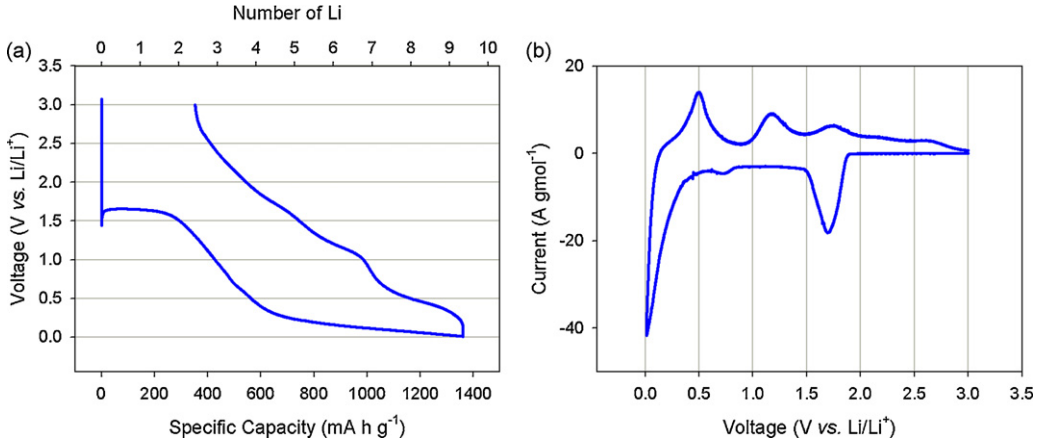

Fig. 1. The galvanostatic discharge–charge voltage profile recorded with $CuGeO_3$/Li cell in the first cycle (a) and cyclic voltammogram (b). Note that the voltage plateaus appeared in (a) are well-matched with the current peaks appeared in (b).

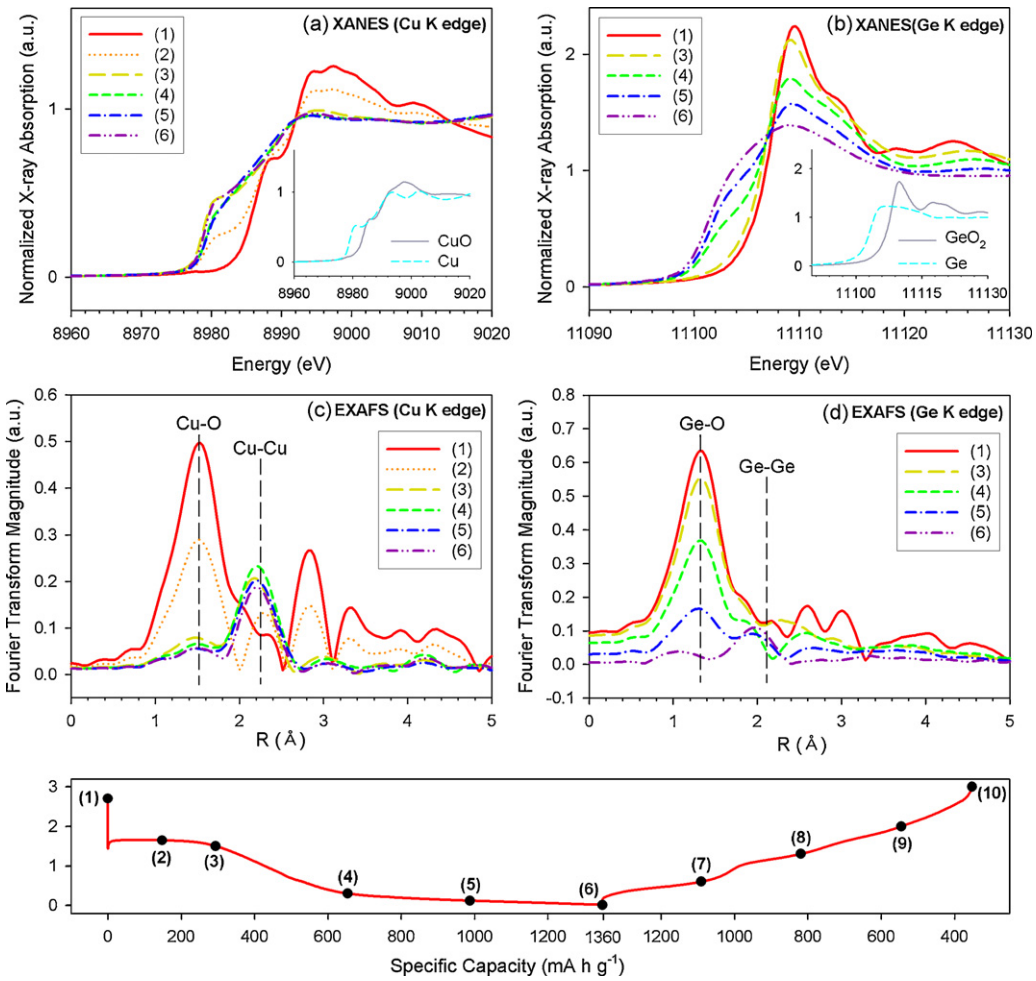

Fig. 2. The X-ray absorption spectra (XAS) obtained with a lithiation of $CuGeO_3$ electrode in the first cycle: XANES of Cu K-edge (a), XANES of Ge K-edge (b), EXAFS of Cu K-edge (c), and EXAFS of Ge K-edge (d). The points where the spectra were taken are indicated as the numbers in the voltage profile shown in the bottom.

lithiation (1.7 V plateau region, scan #1–3) at the expense of Cu–O intensity.

Fig. 2b shows the reduction behavior of Ge component in $CuGeO_3$. The initial $CuGeO_3$ gives a Ge K-edge XANES spectrum (scan #1) that looks close to that of GeO_2 reference, indicating that the oxidation state of Ge in $CuGeO_3$ is close to four. The GeO_2-like spectra are still observed at the voltage plateau region (1.7 V), reflecting that the Ge component is not reduced (scan #1–3) in this voltage region. The Ge reduction takes place at the later stage of lithiation as evidenced by the spectra (scan #4–6) that look similar to that for Ge reference. The EXAFS data (Fig. 2d) further support the later stage Ge reduction. That is, the Ge–O peak intensity does not change at the plateau region (scan #1–3), but rapidly decreases at the later stage (scan #4–6). One revealing feature here is that the intensity of Ge–Ge bonding is very weak even if the Ge component is reduced to its metallic state (scan #4–6 in Fig. 2d), which is contrasted by the relatively strong and invariant peak intensity of Cu–Cu bonding (scan #3–6 in Fig. 2c). This explains that the metallic Ge generated by the conversion reaction immediately reacts with Li by alloying reaction to be lithiated Ge (Li_xGe), whereas the metallic Cu remains as a metallic state without any reactions. By summarizing the above results, the lithiation mechanism of $CuGeO_3$ is proposed as follows:

(i) Cu reduction at the plateau region (1.7 V):

$$CuGeO_3 + 2Li^+ + 2e^- \rightarrow Cu + Li_2O + GeO_2$$

(ii) Ge reduction and alloying reaction at <1.7 V:

$$GeO_2 + 4Li^+ + 4e^- \rightarrow Ge + 2Li_2O$$

and

$$Ge + xLi^+ + xe^- \rightarrow Li_xGe$$

On the basis of this lithiation pathway, the current peaks located at 1.7 V and 0.0 V (Fig. 1b) can be assigned to being associated with the Cu reduction and Ge reduction/alloying, respectively.

The de-lithiation mechanism of $CuGeO_3$ electrode can be addressed by the XAS data shown in Fig. 3. The Cu K-edge XANES spectra (Fig. 3a) look very close to that for the Cu reference (inset in Fig. 2a) regardless of the extent of de-lithiation, indicating that the Cu component maintains its metallic state in this oxidizing condition. This feature is further supported by the strong and invariant Cu–Cu peak in the EXAFS data (Fig. 3c) in the whole period of de-lithiation. A slight Cu oxidation seems likely at the extremely positive potential (>2.5 V) as evidenced by the evolution of Cu–O peak at the final stage of de-lithiation (scan #10 in Fig. 3c). Fig. 3b presents the Ge K-edge XANES spectra, where it is seen that the spectra taken in the earlier period of de-lithiation (<1.0 V, scan #6–7) look like that for Ge reference, but the GeO_2-like spectra gradually develop at the later stage of de-lithiation (>1.0 V). This illustrates that the de-lithiation proceeds in two steps; de-alloying

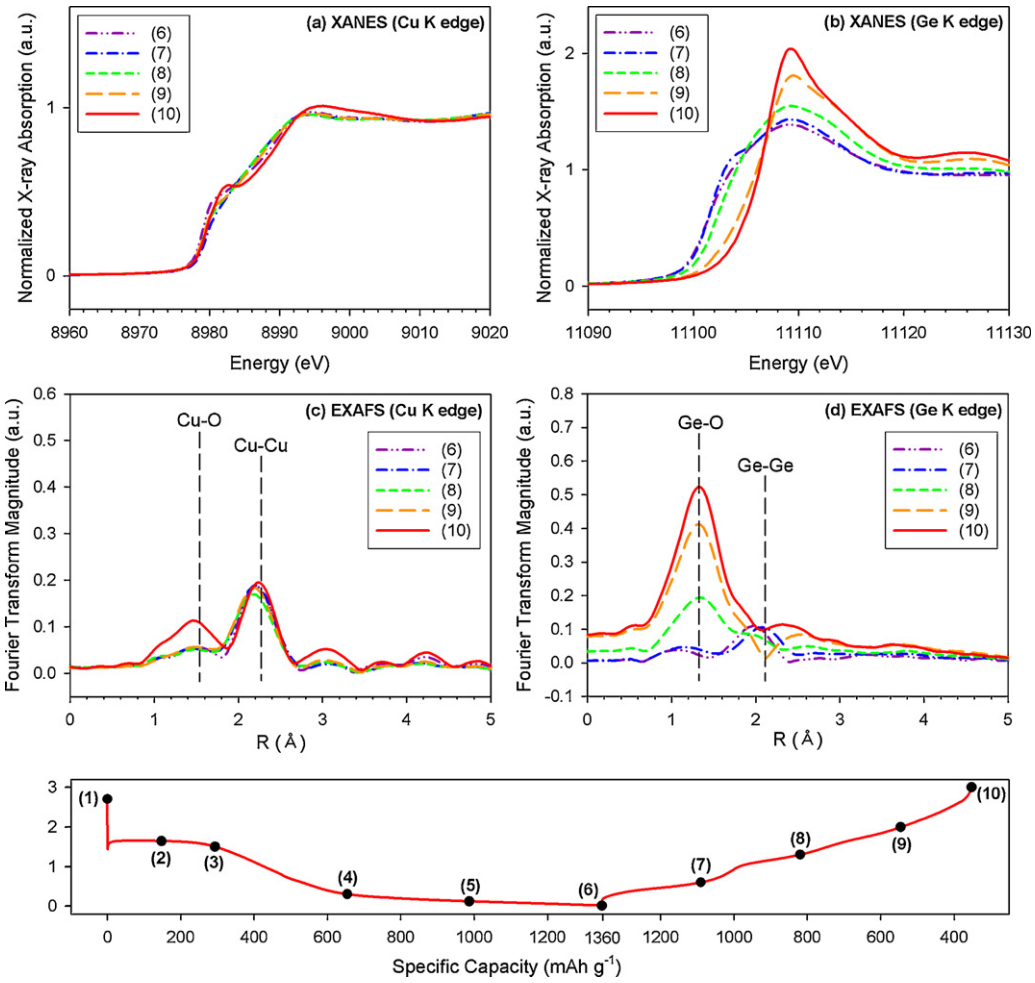

Fig. 3. The X-ray absorption spectra (XAS) obtained with a de-lithiation of $CuGeO_3$ electrode in the first cycle: XANES of Cu K-edge (a), XANES of Ge K-edge (b), EXAFS of Cu K-edge (c), and EXAFS of Ge K-edge (d). The points where the spectra were taken are indicated as the numbers in the voltage profile shown in the bottom.

and then Ge oxidation. The later stage Ge oxidation is further supported by the EXAFS spectra (Fig. 3d), where it is seen that the peak for Ge–O bond, which is negligible in intensity on the spectra #6–7, now becomes more intense on the spectra #8–10. The de-lithiation mechanism of $CuGeO_3$ electrode is summarized as follows:

(i) De-alloying reaction at <1.0 V:

$$Li_xGe \rightarrow Ge + xLi^+ + xe^-$$

(ii) Ge oxidation at >1.0 V:

$$Ge + 2Li_2O \rightarrow GeO_2 + 2Li^+ + 2e^-$$

According to this de-lithiation pathway, the current peak at 0.5 V (Fig. 1b) can be assigned to the de-alloying reaction of Li_xGe, and those at 1.2 V and 1.8 V to Ge oxidation.

Fig. 4a and b shows the first discharge–charge voltage profile taken with the GeO_2/Li cell and the cyclic voltammogram, respectively. The GeO_2 electrode accepts *ca.* 8.3 Li/Ge under this cycling condition. Assuming that GeO_2 is lithiated by a conversion reaction with 4.0 Li/Ge uptake, the extra lithiation capacity (4.3 Li/Ge uptake) can be ascribed to being originated from Li–Ge alloying reaction [5]. The observed de-lithiation capacity is much smaller than the lithiation capacity, such that the coulombic efficiency in the first cycle amounts to only 43%. Note that this value is far smaller than that observed with the Cu-containing $CuGeO_3$ electrode (74%). The reason for why the GeO_2 electrode exhibits such a low coulombic efficiency can be found from the de-lithiation behavior shown in Fig. 4a and b. Two voltage plateaus are observed in the de-lithiation curve (Fig. 4a), which are closely associated with the current peaks appeared at 0.45 V and 1.1 V in the cyclic voltammogram (Fig. 4b). On the basis of the de-lithiation behavior of Ge component in $CuGeO_3$ electrode that has been explained by the XAS data (Fig. 3b and d), the voltage plateau at 0.45 V can be accounted for by the de-alloying reaction, while the plateau appeared at 1.1 V by Ge oxidation. Here, it is noted that the de-lithiation capacity delivered by Ge oxidation (1.1 V plateau) is much smaller than that for de-alloying (0.45 V plateau). Moreover, a comparison for $CuGeO_3$ (Fig. 1a) and GeO_2 electrode (Fig. 4a) clearly shows that the de-lithiation capacity delivered by Ge oxidation at >1.0 V is much smaller for the GeO_2 electrode. From this, we can reach a conclusion that the poor coulombic efficiency observed with the GeO_2 electrode is mainly caused by a poor kinetics for Ge oxidation.

Fig. 4c and d displays the first discharge–charge voltage profile of CuO/Li cell and cyclic voltammogram, respectively. The CuO electrode is lithiated by *ca.* 3.0 Li/Cu, which is larger than the theoretical value (2.0 Li/Cu for conversion reaction) [2]. This extra capacity may be resulted from the reversible formation/decomposition of an organic layer [15] or the capacitor-like charge storage in the newly formed Li_2O/Cu grain boundaries [16]. The latter possibility is supported by the sloped voltage profile appeared in the later stage of lithiation (0.8–0.01 V) and earlier stage of de-lithiation (0.01–2.0 V)

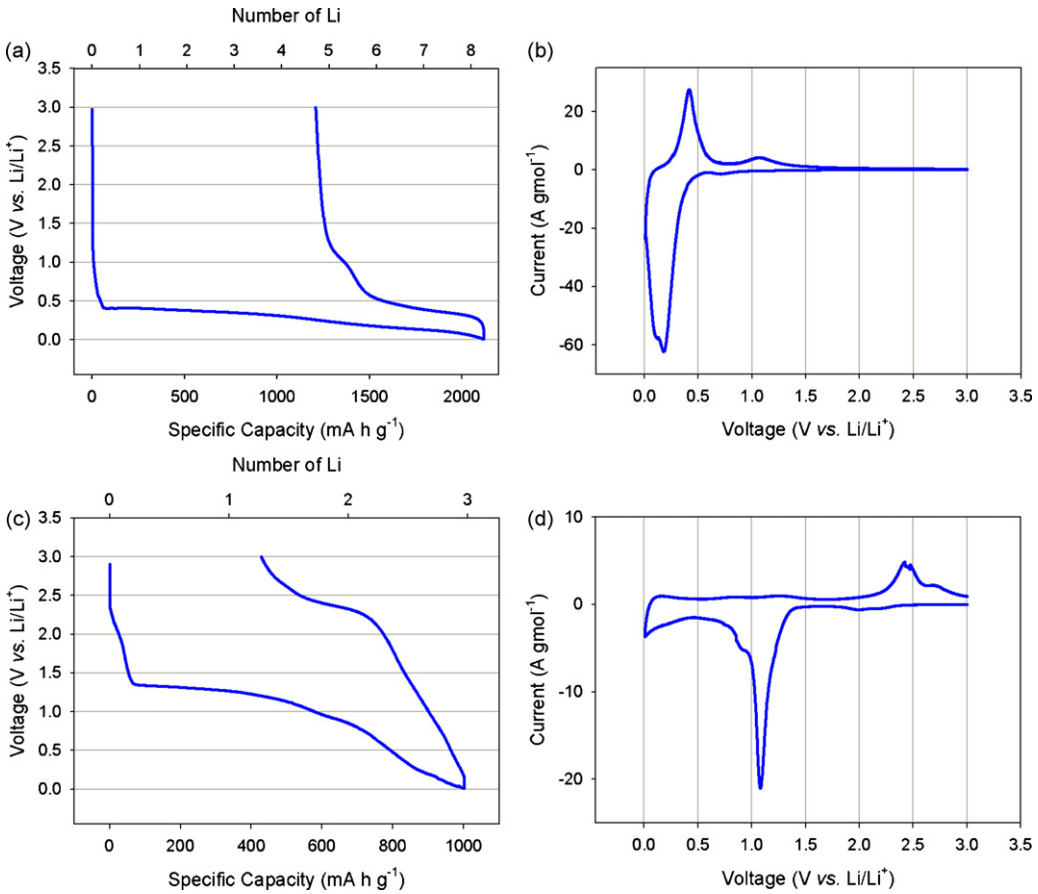

Fig. 4. The galvanostatic discharge–charge voltage profile recorded with GeO_2/Li (a) and CuO/Li (c) cells and cyclic voltammograms (b and d).

in Fig. 4c, and the capacitor-like charging current appeared in the same voltage region in the cyclic voltammogram (Fig. 4d). The current peak and voltage plateau appeared at 1.3–0.8 V in both figures must be ascribed to the conversion-type lithiation reaction, whereas those appeared at 2.3–2.7 V in the de-lithiation period to Cu oxidation. The Cu oxidation at the extremely positive potential (>2.5 V) has been proposed in the XAS study (Fig. 3c).

3.2. The role of nano-dispersed metallic Cu

The discharge/charge voltage curves shown in Figs. 1 and 4 strongly indicate that the voltage profile of $CuGeO_3$ electrode is a combined one of those for CuO and GeO_2. That is, the voltage plateau at 1.7 V in the lithiation curve looks similar to that appeared in CuO electrode and the other plateau at 0.5–0.0 V to that for GeO_2. This may suggest that the Cu and Ge component in $CuGeO_3$ behave independently to each other. Even this, it is clearly shown above that the first coulombic efficiency of Ge component in $CuGeO_3$ is greatly improved by the presence of Cu component, which is mainly indebted to a significant enlargement of de-lithiation capacity delivered by Ge oxidation. This implies that the *in situ* generated metallic Cu plays a favorable role for the Ge oxidation reaction.

Before addressing the role of metallic Cu particles, their size and dispersion in the electrode layer were examined by post-mortem XRD analysis. Fig. 5 presents the XRD patterns of $CuGeO_3$ electrode taken along with a cycling. The initial $CuGeO_3$ powder shows a highly crystalline orthorhombic lattice, indicating that it is not a physical mixture of CuO and GeO_2. When the electrode is lithiated up to 300 mAh g^{-1} (just beyond the plateau region at 1.7 V in Fig. 1a), however, the electrode gives a featureless XRD pattern. Any crystalline phases are not detected in the subsequent cycling,

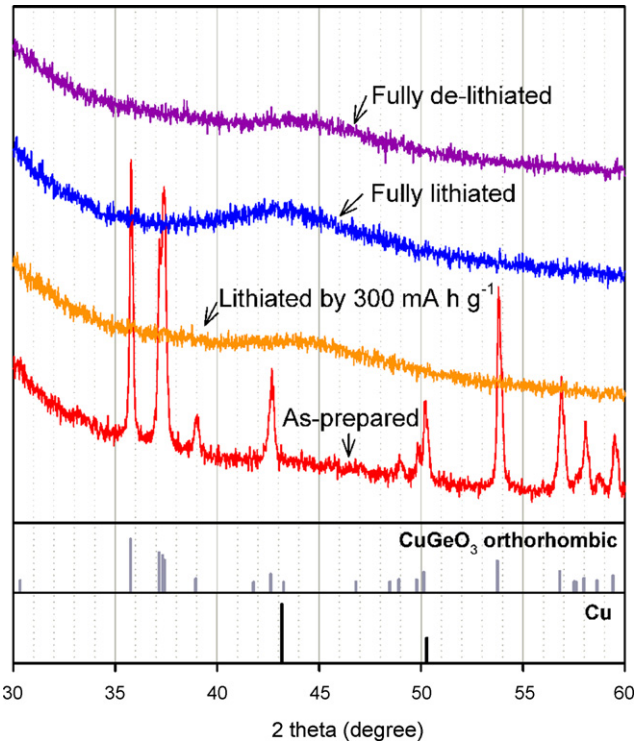

Fig. 5. The *ex situ* XRD patterns of $CuGeO_3$ electrode obtained in the first cycle. Note that the broad peak at 30–35° comes from polyimide (KAPTON) film. Also note that the $CuGeO_3$ phase is converted to amorphous or extremely small particles upon lithiation and any highly crystalline phases are not detected thereafter.

reflecting that the intermediate phases generated during cycling such as metallic Cu, metallic Ge, lithiated Ge, and GeO_2 are amorphous or extremely small in particle size. A broad peak locating at 43–45° can, however, be recognized in all the data, which seems to come from metallic Cu. This is not surprising since a transformation from crystalline to nano-sized amorphous phases is a common feature in the metal oxide electrodes that undergo a conversion reaction [1–4].

As presented in the Section 1, the previous literatures reported an improvement of coulombic efficiency by incorporating extra metal particles in metal oxide electrodes (for instance, Ni/Co_3O_4) [10]. The efficiency improvement has been attributed to a facilitation of Co oxidation reaction. In this work, a similar effect has been obtained by adding a Cu component in the metal oxide (GeO_2) as a form of $CuGeO_3$ (Fig. 1a). Intuitively, the facilitation of Ge oxidation (Li_2O decomposition) must be resulted from a rate improvement in several processes involved for Ge oxidation ($Ge + 2Li_2O \rightarrow GeO_2 + 2Li^+ + 2e^-$); Li_2O decomposition and electron/ion transfer. Several roles for metallic Cu can thus be assumed: The metallic Cu particles may act as an electrocatalyst for Li_2O decomposition. Also, they may play as an electron transfer channel by making an intimate contact with Ge and Li_2O nanoparticles. Finally, they may play as a buffer against volume change evolved with lithiation/de-lithiation of Ge component in $CuGeO_3$. If this is not the case, ion (Li^+ and O^{2-}) transfer between Ge and Li_2O particles may be impeded due to extended inter-particle gaps in the loosened electrode layer.

The above-mentioned assumptions are, however, not easy to be experimentally validated as many ingredients are involved with many interfaces. It is even more difficult to identify which contribution is dominant over the others. Along this line, in this work, the role of Cu particles has been addressed by estimating the electrode polarization that reflects the sum of ohmic resistance, charge transfer resistance and mass transfer resistance for electrode reactions. Fig. 6a provides a typical galvanostatic intermittent titration technique (GITT) data that was obtained with the $CuGeO_3$ electrode, wherein the open circles represent the open-circuit voltage (OCV) and the solid line the transient one [17]. The difference between two values is the electrode polarization that reflects the internal resistance of $CuGeO_3$ electrode [18,19]. Fig. 6b compares the potential-dependant polarization for three electrodes, which was traced along with de-lithiation. The electrode polarization is comparable for three electrodes at <1.0 V, where the de-alloying reaction takes place. In the Ge oxidation region (>1.0 V), however, the GeO_2 electrode shows the largest polarization but the $CuGeO_3$ electrode the smallest. Clearly, the electrode polarization that reflects the Ge oxidation kinetics is greatly reduced by the presence of metallic Cu in the $CuGeO_3$ electrode. Also shown in Fig. 6b is the electrode polarization for the CuO/GeO_2 mixture electrode, which was prepared by ball-milling. This electrode also shows a reduced electrode polarization as compared to the GeO_2 electrode, but the polarization is still larger than that for $CuGeO_3$. It is not difficult to assume that the CuO in CuO/GeO_2 electrode is reduced to metallic Cu and plays the same favorable roles. A slightly larger polarization for this electrode can be explained by the particle size. That is, the particles of CuO and GeO_2 are micron-sized in the initial state, such that even if nano-sized metallic Cu, Ge and Li_2O are generated by lithiation, the contact area between the ingredients (for instance, between Cu and Ge particles) is not large as compared to that formed in the $CuGeO_3$ electrode, wherein the nano-sized metallic Cu, Ge and Li_2O make an intimate contact to each other since they are generated within a single $CuGeO_3$ particle. In the latter circumstance, it is very likely that the nano-sized metallic Cu plays the above-mentioned roles more effectively.

Table 1 lists the lithiation/de-lithiation capacity and coulombic efficiency in the first cycle. The values listed in the top three

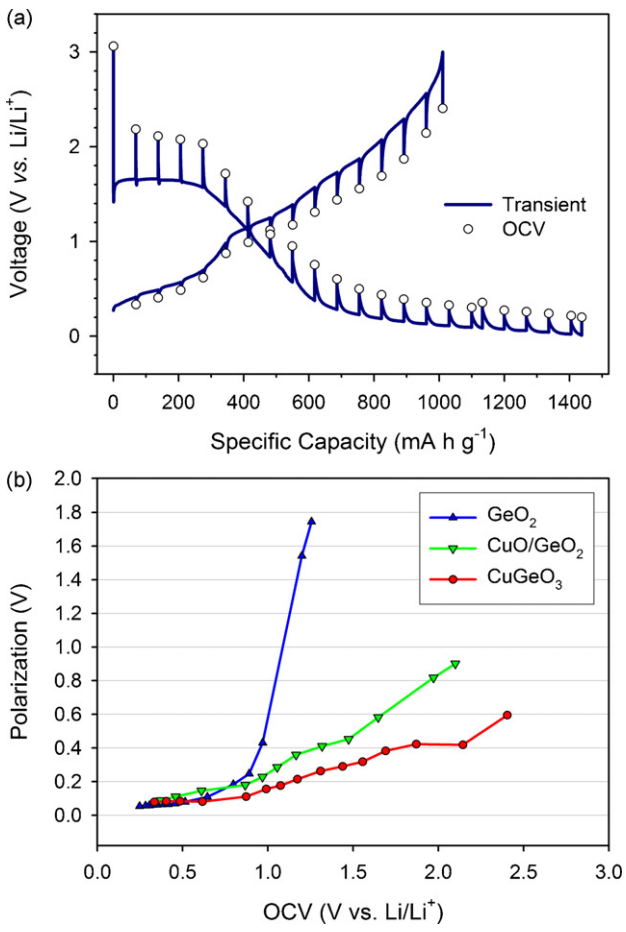

Fig. 6. The GITT profile obtained with $CuGeO_3$/Li cell (a). The transient profile was obtained at a current density of 100 mA g^{-1}, whereas the open-circuit voltage (OCV) was obtained after a rest for 10 h. The electrode polarization obtained with the GeO_2, CuO/GeO_2, and $CuGeO_3$ electrodes in the de-lithiation period (b).

columns reveal that the coulombic efficiency has an inverse relation with the electrode polarization (Fig. 6b), reflecting once again that the Ge oxidation kinetics is the decisive factor in controlling the coulombic efficiency. Also presented in Table 1 is the coulombic efficiency observed with the other ternary oxides; $FeGeO_3$ and $CoGeO_3$. They also exhibit a higher coulombic efficiency than that for GeO_2 electrode. In these systems, it is expected that the reduction of Fe and Co components upon lithiation is advanced before Ge reduction [14], such that the same roles to the metallic Cu in $CuGeO_3$ electrode can be assumed. Finally, even if the coulombic efficiency of $CuGeO_3$ electrode is markedly enhanced as compared to that for GeO_2 electrode, its cycle performance is not highly promising since the capacity steadily decreases. Both electrodes show a severe capacity fading by delivering 50% of the initial value within 20 cycles. This unsatisfactory observation is seemingly come from the intrinsic property of GeO_2, which cannot be overcome by the presence of metallic Cu. That is, one can expect a detachment of

Table 1
The lithiation/de-lithiation capacity and coulombic efficiency in the first cycle.

	Lithiation capacity (mA h g^{-1})	De-lithiation capacity (mA h g^{-1})	Coulombic efficiency (%)
GeO_2	2117	908	42.9
CuO/GeO_2	1485	949	63.9
$CuGeO_3$	1360	1007	74.0
$FeGeO_3$	1456	1038	71.3
$CoGeO_3$	1334	932	69.9

materials from the current collector that is induced by a severe volume change of GeO_2 and/or dissolution of materials into electrolyte [5,20].

4. Conclusion

In this work, we tried to *in situ* generate nano-sized metallic Cu by reducing a Cu-containing oxide electrode ($CuGeO_3$). It was found that the nano-sized metallic Cu particles are indeed generated and they facilitate the Ge oxidation (Li_2O decomposition), such that the first coulombic efficiency is greatly improved as compared to that for the Cu-absent GeO_2 electrode. The following points are summarized:

(i) Upon lithiation, the Cu component in $CuGeO_3$ is reduced earlier than the Ge component and remains as a metallic state thereafter. Owing to the presence of metallic Cu in the $CuGeO_3$ electrode, the electrode polarization in the Ge oxidation region (>1.0 V) is significantly decreased, thereby the de-lithiation capacity delivered by Ge oxidation is greatly enhanced.

(ii) The CuO/GeO_2 mixture electrode, wherein the generation of nano-sized metallic Cu is also assumed, still exhibits a larger polarization than the $CuGeO_3$ electrode in the Ge oxidation region. In the latter electrode, Cu particles are generated within a $CuGeO_3$ grain, such that they make an intimate contact with the other lithiation products (nano-sized Ge and Li_2O particles). In the mixture electrode, however, the contact area seems to be smaller since the Cu and Ge particles are generated separately within a few-micron-sized CuO and GeO_2 grain, respectively. Accordingly, the metallic Cu formed in the $CuGeO_3$ electrode plays the proposed roles (electrocatalyst for Li_2O decomposition, electronic conductive network formation with Ge and Li_2O particles, and buffer against electrode swelling) more effectively than those formed in the CuO/GeO_2 mixture electrode.

Acknowledgements

This work was supported by WCU program through KOSEF funded by the Ministry of Education, Science and Technology (400-2008-0230). The authors also wish to acknowledge the Research Center for Energy Conversion and Storage for financial support, and the Pohang Light Source (PLS) for the XAS measurements.

References

[1] P. Poizot, S. Laruelle, S. Grugeon, L. Dupont, J.M. Tarascon, Nature 407 (2000) 496.
[2] A. Débart, L. Dupont, P. Poizot, J.B. Leriche, J.M. Tarascon, J. Electrochem. Soc. 148 (2001) A1266.
[3] D. Larcher, C. Masquelier, D. Bonnin, Y. Chabre, V. Masson, J.B. Leriche, J.M. Tarascon, J. Electrochem. Soc. 150 (2003) A133.
[4] I.A. Coutney, J.R. Dahn, J. Electrochem. Soc. 144 (1997) 2045.
[5] J.S. Peña, I. Sandu, O. Joubert, F.S. Pascual, C.O. Areán, T. Brousse, Electrochem. Solid-State Lett. 7 (2004) A278.
[6] H. Li, P. Balaya, J. Maier, J. Electrochem. Soc. 151 (2004) A1878.
[7] J. Christensen, J. Newman, J. Electrochem. Soc. 152 (2005) A818.
[8] S.C. Nam, Y.S. Yoon, W.I. Cho, B.W. Cho, H.S. Chun, K.S. Yun, J. Electrochem. Soc. 148 (2001) A220.
[9] P. Limthongkul, H. Wang, Y.M. Chiang, Chem. Mater. 13 (2001) 2397.
[10] Y.M. Kang, K.T. Kim, K.Y. Lee, S.J. Lee, J.H. Jung, J.Y. Lee, J. Electrochem. Soc. 150 (2003) A1538.
[11] X.H. Huang, J.P. Tu, B. Zhang, C.Q. Zhang, Y. Li, Y.F. Yuan, H.M. Wu, J. Power Sources 161 (2006) 541.
[12] C.Q. Zhang, J.P. Tu, Y.F. Yuan, X.H. Huang, X.T. Chen, F. Mao, J. Electrochem. Soc. 154 (2007) A65.
[13] Y. Sharma, N. Sharma, G.V.S. Rao, B.V.R. Chowdari, Adv. Funct. Mater. 17 (2007) 2855.
[14] P. Poizot, S. Laruelle, S. Grugeon, J.M. Tarascon, J. Electrochem. Soc. 149 (2002) A1212.
[15] S. Laruelle, S. Grugeon, P. Poizot, M. Dollé, L. Dupont, J.M. Tarascon, J. Electrochem. Soc. 149 (2002) A627.
[16] Y.F. Zhukovskii, P. Balaya, E.A. Kotomin, J. Maier, Phys. Rev. Lett. 96 (2006) 058302.
[17] W. Weppner, R.A. Huggins, J. Electrochem. Soc. 124 (1977) 1569.
[18] Y.S. Jung, K.T. Lee, J.H. Ryu, D. Im, S.M. Oh, J. Electrochem. Soc. 152 (2005) A1452.
[19] J.H. Ryu, J.W. Kim, Y.E. Sung, S.M. Oh, Electrochem. Solid-State Lett. 7 (2004) A306.
[20] P. Arora, R.E. White, M. Doyle, J. Electrochem. Soc. 145 (1998) 3647.